Electronic State-Selected Reactivity of Transition Metal Ions: Co^+ and Fe^+ with Propane

Petra A. M. van Koppen,* P. R. Kemper, and Michael T. Bowers*

Contribution from the Department of Chemistry, University of California, Santa Barbara, California 93106. *Received July 13, 1992*

Abstract: Recently, we developed a "chromatographic" technique to determine the electronic state distribution for transition metal ions. This method allows the study of state-selected reactions. In this paper we report the quantitative determination of rate constants and branching ratios for state-selected Co^+ and Fe^+ reacting with propane. Observed rates for adduct formation as well as H_2 and CH_4 elimination channels were strongly dependent on the electronic configuration of the metal ion. Co^+ ions were formed by electron impact on either $Co(CO)_3NO$ or $CoCp(CO)_2$ or by surface ionization of $CoCl_2$. The Co^+ electronic state population is a function of both the electron energy and the precursor used, and can be varied from 36% ground state to 97% ground state. Thus, we can measure reaction rate constants over a wide range of ground- and excited-state populations and extrapolate to 100% ground- or excited-state Co^+ to obtain the state-specific reaction rates. Under our experimental conditions (10^{-5} Torr of C_3H_8 in 1.75 Torr of He), adduct formation is the dominant product for the a^3F $3d^8$ ground state of Co^+, with only small amounts of elimination products observed. The $4s3d^7$ excited states (a^5F and b^3F) show greatly reduced clustering (due to the repulsive 4s electron) and enhanced elimination channels. Fe^+ was formed by electron impact on $Fe(CO)_5$. Again the electronic state population was varied by varying the electron energy. Absolute rate constants were obtained for the ^6D ground state as well as for the ^4F and ^4D excited states of Fe^+ reacting with C_3H_8. Adduct formation is the dominant product for the ^6D $4s3d^6$ ground state of Fe^+ despite the repulsive 4s electron. This is due to a crossing from the ground-state surface to the $Fe^+(^4F\ 3d^7)C_3H_8$ first excited-state surface where the adduct is more strongly bound. The Fe^+ ^4D $4s3d^6$ second excited state reacts similarly to the Co^+ a^5F and b^3F $4s3d^7$ excited states.

Introduction

Probing the kinetics, dynamics, and thermochemistry of organo-transition-metal reactions using mass spectrometric techniques has shown these reactions to be complex[1,2] and usually extremely dependent on the metal ion electronic state.[3-12] It is therefore important to carry out state-selected reactivity studies. Radiative lifetimes of excited-state metal ions are long (on the order of seconds) owing to parity forbidden transitions.[13] Consequently, once the excited electronic states are produced, their reactivity can be studied provided the state can be selected. The electronic state configurations and corresponding energies for Co^+ and Fe^+ are summarized in Table I.[14] Atomic transition metal ions produced by electron impact,[3] surface ionization,[6,15-17] or laser vaporation[17,18] are formed in a mixture of ground and excited states. With electron impact (EI) the excited electronic state population is a strong function of the electron energy, increasing rapidly with increasing electron energy up to 40-50 eV. Laser vaporization also produces a significant amount of electronically excited ions. With surface ionization (SI), a Boltzmann distribution of ground and excited states is produced. Only with resonant multiphoton ionization (REMPI)[4,5,19] can pure ground- and excited-state metal ions be produced. REMPI is limited, however, owing to the complexity and difficulty associated with this technique.

Table I. Electronic States of Fe^+ and Co^+

ion	state	configuration	energy[a] (eV)
Fe^+	a^6D	$4s3d^6$	0.052
	a^4F	$3d^7$	0.300
	a^4D	$4s3d^6$	1.032
	a^4P	$3d^7$	1.688
	a^2G	$3d^7$	1.993
Co^+	a^3F	$3d^8$	0.086
	a^5F	$4s3d^7$	0.515
	b^3F	$4s3d^7$	1.298
	a^1D	$3d^8$	1.445
	a^3P	$3d^8$	1.655

[a] Reference 14; averaged over J levels.

Recently, we developed a simple way to characterize populations of electronically excited metal ions using a "chromatographic" technique.[3,20] The valence electron configurations for atomic transition metal ions, which are $3d^n$ or $4s3d^{n-1}$, exhibit large differences in mobility. These differences in mobility give rise to a spatial and temporal spread of the metal ions in different electronic states as they diffuse through a buffer gas. If a mass-selected ion beam is pulsed into the reaction cell containing

(1) For a recent review, see: Eller, K.; Schwarz, H. *Chem. Rev.* **1991**, *91*, 1121 and references therein.
(2) *Gas Phase Inorganic Chemistry*; Russel, D. H., Ed.; Plenum Press: New York, 1989.
(3) (a) Kemper, P. R.; Bowers, M. T. *J. Phys. Chem.* **1991**, *95*, 5134. (b) Kemper, P. R.; Bowers, M. T. *J. Am. Chem. Soc.* **1990**, *112*, 3231.
(4) Weisshaar, J. C. In *Advances in Chemical Physics*; Ng, C., Ed.; Wiley-Interscience: New York, 1992; Vol. 81 and references therein.
(5) Sanders, L.; Hanton, S.; Weisshaar, J. C. *J. Phys. Chem.* **1987**, *91*, 5145. Sanders, L.; Hanton, S. D.; Weisshaar, J. C. *J. Chem. Phys.* **1990**, *92*, 3498.
(6) Armentrout, P. B. *Annu. Rev. Phys. Chem.* **1990**, *41*, 313 and references therein.
(7) Armentrout, P. B. In *Gas Phase Inorganic Chemistry*; Russell, D. H., Ed.; Plenum Press: New York, 1989.
(8) Freas, R. B.; Ridge, D. P. *J. Am. Chem. Soc.* **1980**, *102*, 7129. Reents, W. D., Jr.; Strobel, F.; Freas, R. B., III; Ridge, D. P. *J. Phys. Chem.* **1985**, *89*, 5666.
(9) Halle, L. F.; Armentrout, P. B.; Beauchamp, J. L. *J. Am. Chem. Soc.* **1981**, *103*, 962.
(10) Elkind, J. L.; Armentrout, P. B. *J. Phys. Chem.* **1986**, *90*, 5736.
(11) Elkind, J. L.; Armentrout, P. B. *J. Phys. Chem.* **1987**, *91*, 2037.
(12) (a) Sunderlin, L. S.; Aristov, N.; Armentrout, P. B. *J. Am. Chem. Soc.* **1987**, *109*, 78. (b) Aristov, N.; Armentrout, P. B. *J. Am. Chem. Soc.* **1986**, *108*, 1806.
(13) Garstang, R. H. *Mont. Not. R. Astron. Soc.* **1962**, *124*, 321.
(14) (a) Moore, C. E. *Atomic Energy Levels*; U.S. National Bureau of Standards: Washington, DC, 1952; Circ. 467 (U.S. National Bureau of Standards). (b) Sugar, J.; Corliss, C. *J. Phys. Chem. Ref. Data* **1981**, *10*, 197, 1097. (c) Sugar, J.; Corliss, C. *J. Phys. Chem. Ref. Data* **1982**, *11*, 135.
(15) Sunderlin, L. S.; Armentrout, P. B. *J. Phys. Chem.* **1988**, *92*, 1209.
(16) Schultz, R. H.; Elkind, J. L.; Armentrout, P. B. *J. Am. Chem. Soc.* **1988**, *110*, 411.
(17) Loh, S. K.; Fisher, E. R.; Lian, Li; Schultz, R. H.; Armentrout, P. B. *J. Phys. Chem.* **1989**, *93*, 3159.
(18) Cody, R. B.; Burnier, R. C.; Reents, W. D., Jr.; Carlin, T. J.; McCrery, D. A.; Lengel, R. K.; Freiser, B. S. *Int. J. Mass Spectrom. Ion Phys.* **1980**, *33*, 37.
(19) Hanton, S. D.; Noll, R. J.; Weisshaar, J. C. *J. Phys. Chem.* **1990**, *94*, 5655.
(20) Kemper, P. R.; Bowers, M. T. *J. Am. Soc. Mass Spectrom.* **1990**, *1*, 197.

0002-7863/92/1514-10941$03.00/0

a buffer gas, ions with different electronic configurations separate as they diffuse through the cell and are observed at different times in the arrival time spectrum. The excited- and ground-state populations can be determined by integrating the corresponding peak areas. The electronic state population is a function of both the electron energy and the neutral precursor used and can be varied over a wide range. Reaction rate constants are measured as a function of the percent ground and excited state to obtain the state-selected rate constants for reaction (by extrapolation to 100% ground- and excited-state M^+).[21]

In this paper we will use this technique to determine the reactivity of ground and excited states of Co^+ and Fe^+ with propane. We report the quantitative determination of rate constants for all the observed products which include adduct formation as well as H_2, CH_4, and C_2H_5 elimination channels. The implications of these results on the potential energy surfaces will be discussed.

Experimental Section

Details of the instrument used in these experiments have been described[20] and are only briefly outlined here. The instrument used coupled a reverse-geometry mass spectrometry operating at 5 kV to a high-pressure, temperature-variable drift cell that operates at thermal energies. The first-stage mass spectrometer is a home-built instrument with the same dimensions and ion optics as a V.G. Instruments ZAB-2F. The ion source is a standard V.G. Instruments electron impact ionization source. The source was modified to do surface ionization, with a design similar to that of Armentrout and co-workers.[12b] Co^+ and Fe^+ ions are formed by electron impact on $Co(CO)_3NO$ and $CoCp(CO)_2$, or $Fe(CO)_5$, respectively. In addition, Co^+ ions are formed by surface ionization of $CoCl_2$. In the case of Fe^+, the largest isotope is $m/e = 56$ (91.8%) which conicides with the mass of $(CO)_2^+$ or $Fe(CO)_2^{2+}$, at least one of which is also formed by electron impact on $Fe(CO)_5$.[22] As a result, we used the next largest Fe^+ isotope, $m/e = 54$ (5.8%) in all the experiments. Upon exiting the source, the ions are accelerated to 5 kV and mass selected using the double-focusing reverse geometry mass spectrometer. The ions are then decelerated to 2–3 eV kinetic energy and are focused into the high-pressure drift cell containing 1.75 Torr of helium buffer gas. The ions are quickly thermalized by collisions with He and drift through the reaction cell at constant velocity because of the presence of a uniform drift field. Ions react with a trace ($\sim 1 \times 10^{-5}$ Torr) of C_3H_8 present in the He, exit the cell, and are quadrupole mass analyzed and detected. Reaction times typically range from 200 to 600 μs corresponding to drift fields of $E/N \leq 3.5 \times 10^{-17}$ V·cm^2. These fields do not perturb the ion translational temperature more than a few degrees.[20]

The electronic state populations are largely obtained from the ion arrival time distribution (ATD). The ATD for Co^+ or Fe^+ is measured by pulsing the mass-selected ion beam into the drift cell (pulse width $\sim$ 1–3 μs). The pulse simultaneously triggers a time-to-pulse-height converter ramp. Ions that exit the cell are collected as a function of time, giving the arrival time distribution. Ions that have different mobilities have different drift times through the cell and appear as different peaks in the ATD. With Co^+ no excited-state deactivation occurred and the integrated ATD peak areas equal the populations of the electronic configurations. In the Fe^+ case, deactivation does occur, and a fitting of theoretical and experimental ATDs was required to determine the electronic configuration populations (described below). In both the Fe^+ and Co^+ experiments, two states with $4s3d^{n-1}$ configurations were present, and additional information from the reaction was required to determine the state populations. This point is discussed below.

Additional information regarding individual electronic state reactivities is obtained from product ion ATDs. In these experiments the Co^+ or Fe^+ is pulsed into the cell, but a particular product ion is collected instead of the bare metal ion. These product ATDs have separate components corresponding to the reaction of the $3d^n$ or $4s3d^{n-1}$ configurations to form the particular product. This provides a separate, semiquantitative determination of the relative efficiencies with which the M^+ states react to form the product ion. The use of this technique in the Co^+ experiments is discussed below.

The state-specific rate constants are determined by studying the reaction as a function of the state populations. These populations are altered by changing both the electron energy and the precursor used. For example, at 50 eV, electron impact on $Co(CO)_3NO$ produces 36% ground-state Co^+, whereas $CoCp(CO)_2$ produces 83% ground-state Co^+. With the electronic state population determined, $[M^+]/[M^+]_0$ is measured as a function of time to obtain the total rate constant, k_{tot}. We measure k_{tot} as a function of percent ground-state M^+ and extrapolate to 100% ground-state and 100% excited-state M^+ to determine the relative rates of reaction. Product distributions are measured as a function of percent ground-state M^+ to obtain individual rate constants.

The accuracy of the absolute total rate coefficient measurements is estimated to be within ±30%.[20] THe relative rate coefficient measurements, however, are much more accurate (±10%). The pressure of propane was varied from 1 to 4 $\times 10^{-5}$ Torr, yielding rate coefficients unchanged to within ±15%.

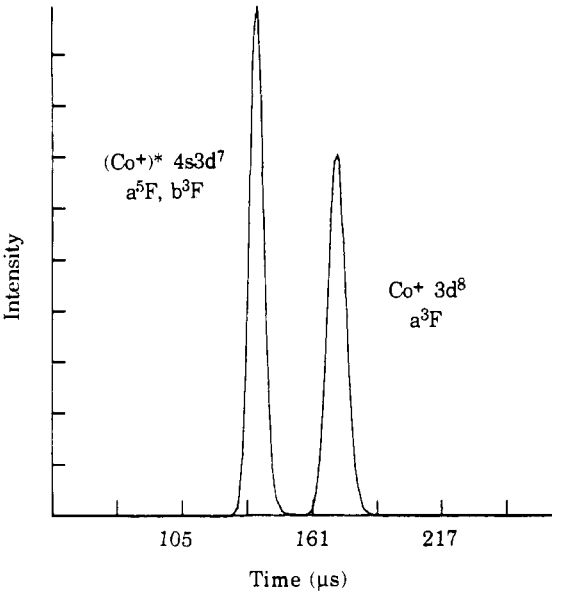

Figure 1. Co^+ arrival time distribution (ATD), 300 K, 50-eV electron energy, Co^+ from $Co(CO)_3NO$. The absence of Co^+ arrival times intermediate between those of the excited and ground state indicates deactivation does not occur from the excited state to the ground state. The integrated peak areas equal the populations of the electronic state configurations.

Results and Discussion

I. Arrival Time Distributions: $Co^+ + C_3H_8$. a. Electronic State Populations. A typical ATD for Co^+ is shown in Figure 1. Two peaks are observed corresponding to ground ($3d^8$) and excited ($4s3d^7$) electronic state configurations. The excited-state Co^+ contains a 4s electron which is larger and more repulsive than the ground state which contains only 3d electrons.[3] The reduced attraction to He gives the excited-state Co^+ a greater mobility than the ground state, causing the excited state to appear earlier in the ATD than the ground state. The two peaks are baseline resolved. The absence of Co^+ arrival times intermediate between those of the excited and ground state indicates deactivation does not occur from the excited state to the ground state, while the ion traverses the reaction cell. Since deactivation does not occur, the integrated ATD peak areas equal the populations of the electronic configurations.

In a recent study[3] of first row transition metal ions, IV–XII, collisional deactivation was observed only for Fe^+ and Mn^+ in He. These are the only cases where an excited state of $3d^n$ configuration was observed to deactivate to a $4s3d^{n-1}$ ground state. Ti^+ also has a $4s3d^{n-1}$ ground- and a $3d^n$ excited-state configuration and has been observed to deactivate by Tonkyn and Weisshaar.[23] The ATD resolution in our previous Ti^+ experiments was insufficient to observe this. In no case did excited $4s3d^{n-1}$ states collisionally deactivate at thermal energies. This finding is nicely explained by a model proposed by Loh et al.[17] Consider the potential curves for a M^+–He collision when the M^+ ground state ion has a $4s3d^{n-1}$

(21) van Koppen, P. A. M.; Kemper, P. R.; Bowers, M. T. *J. Am. Chem. Soc.* **1992**, *114*, 1083.

(22) We observe a doublet in the arrival time distribution for $^{56}Fe^+$. The longer time peak in the doublet is not present for $^{54}Fe^+$. Both short time peaks (for $^{56}Fe^+$ and $^{54}Fe^+$) show tailing to longer times, suggesting deactivation, a point discussed in detail later in this paper. High resolution mass spectra taken by Oriedo and Russell indicate the second peak, (nominal mass $m/e = 56$) is due to the $Fe(CO)_2^{2+}$ impurity (private communication).

(23) Tonkyn, R.; Weisshaar, J. C. *J. Phys. Chem.* **1986**, *90*, 2305.

configuration and the excited state has a $3d^n$ configuration. The $4s3d^{n-1}$ potential energy curve will become repulsive at larger internuclear distance than the $3d^n$ excited configuration, owing to the repulsion between the 4s electron and the filled $1s^2$ shell of He. Thus the potential energy curves for the two states in the collision will cross, perhaps at a low collision energy, providing a means for deactivation in the collision. For $3d^n$ ground states and $4s3d^{n-1}$ excited states, however, the curves will not cross until much higher collision energies, and consequently, excited $4s3d^{n-1}$ configurations should not easily deactivate, as we observe experimentally.

On this basis, the $3d^8$ a^1D and a^3P states of Co^+, which lie only 0.147 eV and 0.357 eV above the $4s3d^7$ b^3F state, respectively, should rapidly collisionally deactivate to the b^3F state. Since such deactivation is not observed in the ATD for Co^+, and a^3P and higher lying excited states are assumed not to be present ($\leq 2\%$) under the high-pressure conditions of our experiment. Consequently, the peak corresponding to the $3d^8$ electronic configuration contains only the ground state. The excited state, however, may be a composite of two states, the a^5F and the b^3F, both of which have $4s3d^7$ electron configurations. Translational energy spectroscopy experiments[24] have confirmed the presence of the b^3F second excited state in Co^+ when formed by electron impact on $Co(CO)_3NO$.[25] No information was obtained regarding the a^5F state.[26] To obtain information regarding the reactivity of the a^5F state with propane, Co^+ was formed by surface ionization of $CoCl_2$. Unlike electron impact, surface ionization of $CoCl_2$ on a resistively heated rhenium ribbon at approximately 2300 K does not have enough energy to form measurable amounts of the b^3F second excited state. The electronic state population obtained by integrating the ATD peak areas is $15 \pm 1\%$ a^5F first excited state and $85 \pm 1\%$ a^3F ground state in agreement with the calculated Boltzmann distribution at this temperature. The a^5F state was found to react with propane at a rate very similar to that of the combined b^3F and a^5F states formed by electron impact (the product ATDs for all channels were the same for Co^+ formed by electron impact and surface ionization; see following section). Consequently, the presence of any a^5F Co^+ formed by electron impact will have a negligible effect on our reported $Co^+(b^3F) + C_3H_8$ rate constants, although the reported fraction of b^3F would be in error.

b. Product Ion Peak Shapes. Product ATDs for the $CoC_3H_8^+$ adduct are shown in Figure 2. Figure 2a shows the ATD for $CoC_3H_8^+$ ions formed in the ion source. The adduct is mass selected and injected into the reaction cell containing only helium. In this case the ATD consists of only one peak. This is due to the fact that the $Co^+C_3H_8$ adduct is much larger than the Co^+ atomic ion, and the resultant differences in the mobility due to different electronic state configurations of Co^+ are negligible. Because of its larger size, the adduct has a lower mobility and shows up at longer times in the ATD (Figure 2a) than either $(Co^+)^*$ or Co^+ (Figure 2c). If Co^+ is injected into the reaction cell, where it reacts with propane to form the adduct, the resulting ATD for the $CoC_3H_8^+$ product ion is broad and has two components as shown in Figure 2b. The arrival time of the adduct is a function of the position at which the reaction took place in the cell. The onset of the $(Co^+)^*C_3H_8$ and $Co^+C_3H_8$ ATDs correlate exactly to the ATDs of $(Co^+)^*$ and Co^+ in Figure 2c, as indicated by the dashed arrows. We interpret this result as follows. If Co^+ reacts with propane at the end of the reaction cell, the arrival time for $CoC_3H_8^+$ formed will correspond to the arrival time of Co^+. The longest arrival times correspond to the ATD of the adduct formed at the entrance of the cell. This corresponds to the ATD of $Co^+C_3H_8$ formed in the ion source (Figure 2a) as shown by the dashed arrow. Ions which react throughout the cell have intermediate arrival times, giving rise to the broad flat-topped peak we observe. The shaded area corresponds to excited-state $(Co^+)^*$ reaction. The shapes of the product ATDs are complicated. However, the calculated ATDs for the $(Co^+)^*C_3H_8$ and $Co^+C_3H_8$, from known transport properties, are expected to be broad and to decrease in intensity at long times. Based on this as well as experimentally observed peak shapes where a single state dominates the reaction, we approximate the peak shape indicated by the shaded area for the $(Co^+)^*C_3H_8$ adduct. Since we have roughly equal amounts of excited- and ground-state Co^+ to start with (48% ground state and 52% excited state), it appears from the relative areas in Figure 2b that ground-state Co^+ forms the adduct far more efficiently than does the excited state. As we increase the percentage of ground-state Co^+ from 48% to 93%, the $(Co^+)^*C_3H_8$ adduct contribution to the ATD essentially disappears.

The product ATD for $CoC_3H_6^+$ (H_2 loss), shown in Figure 3, indicates that this product is produced much more efficiently from the excited state than from the ground state. Starting with 48%

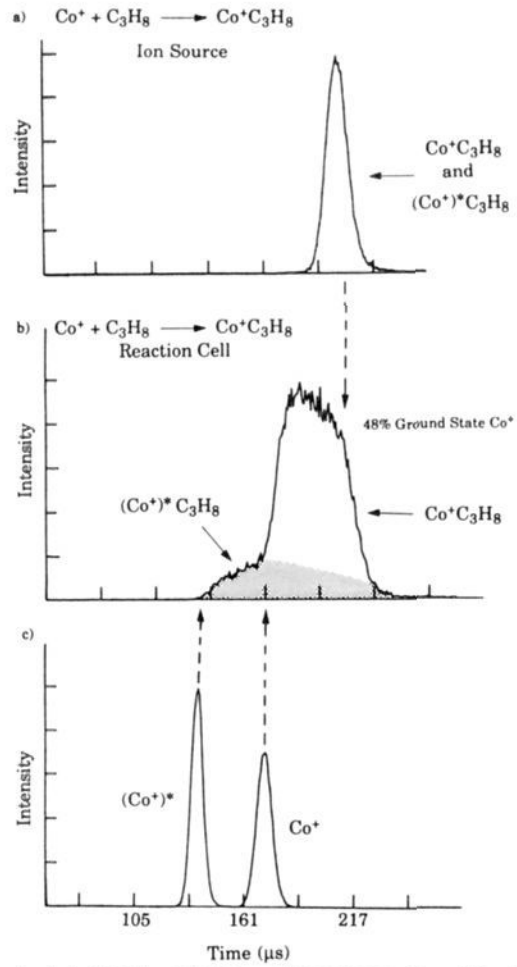

Figure 2. (a) ATD for $Co^+C_3H_8$ and $(Co^+)^*C_3H_8$ formed in the ion source. The adduct is mass selected and injected into the reaction cell. A single peak is observed since $(Co^+)^*C_3H_8$ and $Co^+C_3H_8$ have the same mobility (see text). (b) ATD for $Co^+C_3H_8$ and $(Co^+)^*C_3H_8$ formed in the reaction cell. In this case, the Co^+ ion beam, containing 48% ground-state Co^+ and 52% excited-state $(Co^+)^*$, is injected into the reaction cell where it reacts with propane to form the adduct. The arrival time of the adduct is a function of the position at which the reaction took place in the cell. If Co^+ reacts with propane at the end of the reaction cell, the arrival time for $CoC_3H_8^+$ formed will correspond to the arrival time of Co^+. As a result, the onset of the $(Co^+)^*C_3H_8$ and $Co^+C_3H_8$ ATDs correlate exactly to the ATDs of $(Co^+)^*$ and Co^+, as indicated by the dashed arrows. The longest arrival times correspond to the ATD of the adduct formed at the entrance of the cell. This corresponds to the ATD of $Co^+C_3H_8$ formed in the ion source (a) as shown by the dashed arrow. The shaded area corresponds to excited state $(Co^+)^*$ reaction.

(24) Illies, A. J.; Bowers, M. T. *Chem. Phys.* **1982**, *65*, 281.
(25) Hanratty, M. A.; Beauchamp, J. L.; Illies, A. J.; van Koppen, P. A. M.; Bowers, M. T. *J. Am. Chem. Soc.* **1988**, *110*, 1.
(26) The a^5F state lies only 0.43 eV above the a^3F state (Table I). As a result, it is difficult to resolve these two states using translational energy spectroscopy. With increased resolution, the a^5F state may still not be observed since the $a^5F \leftarrow a^3F$ transition is spin forbidden.

$$Co^+ + C_3H_8 \longrightarrow Co^+C_3H_6 + H_2$$

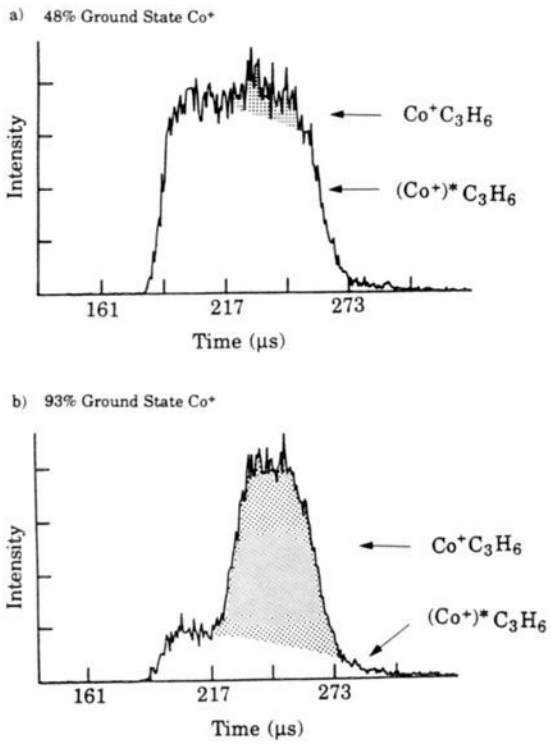

Figure 3. ATDs for $Co^+C_3H_6$ and $(Co^+)^*C_3H_6$ (H_2 loss from the cobalt–propane adduct) formed in the reaction cell. ATDs for (a) 48% and (b) 93% ground-state Co^+ are shown. The shaded area corresponds to ground-state Co^+ reaction. From the relative areas, excited state Co^+ is shown to eliminate H_2 more efficiently than ground state.

$$Co^+ + C_3H_8 \longrightarrow Co^+C_2H_4 + CH_4$$

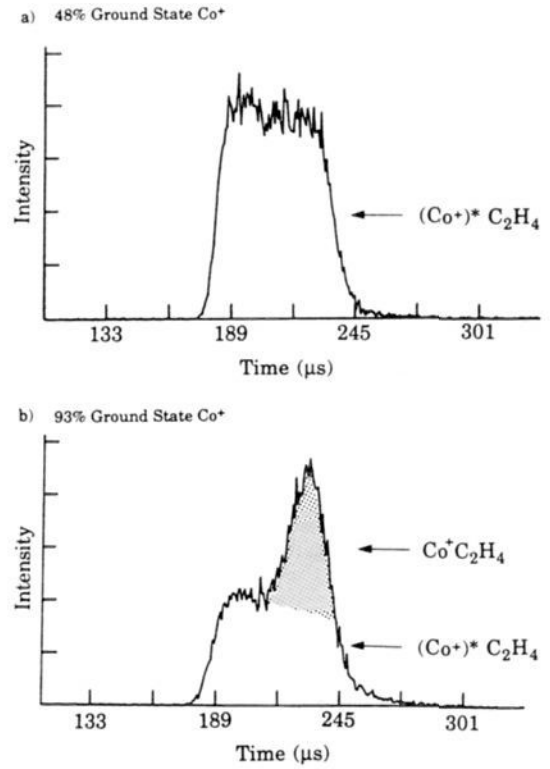

Figure 4. ATDs for $Co^+C_2H_4$ and $(Co^+)^*C_2H_4$ (CH_4 loss from the cobalt–propane adduct) formed in the reaction cell. ATDs for (a) 48% and (b) 93% ground-state Co^+ are shown. The shaded area corresponds to ground-state Co^+ reaction. From the relative areas, excited state Co^+ is shown to eliminate CH_4 more efficiently than ground state.

Scheme I

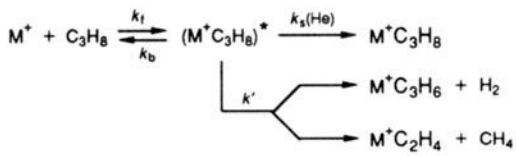

ground-state Co^+ (Figure 3a), the observed contribution to the $CoC_3H_6^+$ ATD from the ground state (the shaded area) is roughly 10%. Starting with 93% ground-state Co^+ (Figure 3b), a significant increase in the ground-state contribution to the $CoC_3H_6^+$ ATD is observed. These results indicate the $(Co^+)^*$ excited state(s) is (are) about five times more efficient at producing $Co^+C_3H_6$ than is the ground state. The product ATD for $CoC_2H_4^+$ (CH_4 loss), Figure 4, is very similar to that of $CoC_3H_6^+$ (H_2 loss). Again the excited state is much more efficient in comparison to ground state in eliminating CH_4.

These experiments give a semiquantitative determination of the relative $Co^+/(Co^+)^*$ efficiencies in forming a given product ion. This result is completely independent of (and complementary to) our kinetic results discussed below.

II. Kinetics: $Co^+ + C_3H_8$. The mechanism assumed for Co^+ reacting with C_3H_8 involves the formation of an internally excited $(Co^+C_3H_8)^*$ complex which can be stabilized by collisions with helium, dissociate back to reactants, or eliminate H_2 or CH_4 (Scheme I). For one electronic state of Co^+, the fractional decrease $Co^+/(Co^+)_0$ is a simple exponential decay:

$$Co^+ = (Co^+)_0 e^{-k_{tot}t} \qquad (1)$$

$$k_{tot} = \frac{k_f k_s(He) + k' k_f}{k_b + k_s(He) + k'}(C_3H_8)$$

There are, however, two electronic states of Co^+ with different reactionrates giving rise to the sum of two exponentials shown in eq 2:

$$Co^+ = f(Co^+)_0 e^{-k_{gs}t} + (1-f)(Co^+)_0 e^{-k_{ex}t} \qquad (2)$$

In this expression, Co^+ corresponds to the sum of ground- and excited-state Co^+, f is the fraction of ground-state Co^+, and k_{gs} and k_{ex} are the ground- and excited-state rate constants, respectively. In the low conversion limit, used in our experiments, the exponential decay of both ground- and excited-state Co^+ is well described by a linear function (i.e., $e^{-kt} \cong 1 - kt$ for $kt \ll 1$). In this case, the sum of the two exponentials in eq 2, effectively reduces to the single exponential decay as given in eq 3:

$$Co^+/(Co^+)_0 = e^{-k_{tot}t} \qquad k_{tot} = fk_{gs} + (1-f)k_{ex} \qquad (3)$$

We obtain k_{tot} by plotting ln $[Co^+/(Co^+)_0]$ versus time. We measure k_{tot} as a function of percent ground-state Co^+ and extrapolate to 100% ground-state Co^+ ($f = 1$) and 100% excited-state Co^+ ($f = 0$) to determine the individual total rates of reaction.[27] Product distributions are measured as a function of percent ground-state Co^+ to obtain individual rate constants.

III. Rates of Reaction: $Co^+ + C_3H_8$. The rate constant for adduct formation is plotted as a function of percent ground-state Co^+ in Figure 5. The experimental data points range from 38 to 96% ground-state Co^+. The linear least-squares fit of the data indicates that for 100% ground-state Co^+ a^3F $3d^8$ the rate of adduct formation is 9.6×10^{-10} cm^3 s^{-1} which is approximately 40 times greater than for the b^3F $4s3d^7$ state.[29] The repulsive

(27) The time used in the analysis corresponds to ground-state Co^+. The extrapolated rate constant for excited-state Co^+ (0% ground state in Figure 5) is corrected for the shorter reaction time for excited-state Co^+. These corrected values are listed in Table II.

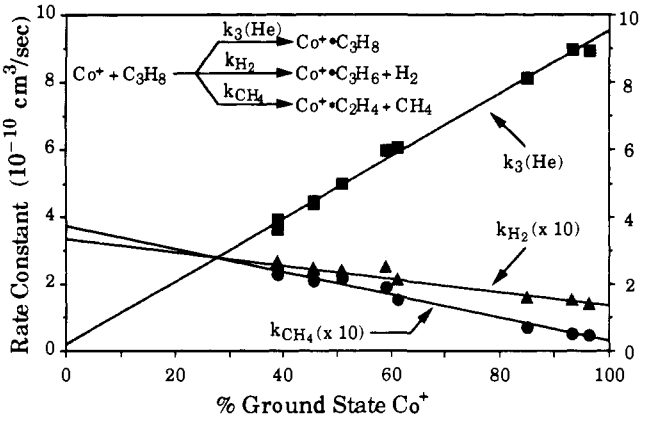

Figure 5. Absolute rate constants for $Co^+C_3H_8$ adduct formation and for H_2 and CH_4 elimination channels as a function of percent ground-state Co^+. The linear least-squares fit of the experimental data points is used to extrapolate to rates of reaction corresponding to 100% ground-state and 100% excited-state Co^+.[27]

4s electron in the Co^+ $4s3d^7$ excited state greatly reduces the depth of the Co^+–C_3H_8 attractive well and is responsible for the reduced clustering efficiency with propane. The factor of 40 difference in the adduct formation rate constants will depend on the pressure of helium since the He pressure dependence of the apparent second-order rate constant differs for the two states. In the high-pressure limit, both ground and excited states will react to form the adduct at the collision rate. However, at 1.75 Torr of helium, the stabilized adduct represents 98% of the ground-state Co^+ products, and the observed rate for adduct formation for the ground state is 82% of the collision limit (i.e., near saturation), whereas the excited state reacts at only 2% of the collision limit (i.e., in the low end of the falloff region). These results are in good agreement with those of Tonkyn et al.[30] for Co^+ reacting with propane at 300 K and 0.75 Torr of He where they found the collisionally stabilized adduct to be the major product (95%) formed at 79% of the collision limit.

Under the high-pressure condition in our experiment (1.75 Torr of He), the H_2 and CH_4 elimination channels are approximately two orders of magnitude smaller than the rate of adduct formation. This inefficient H_2 and CH_4 elimination for ground-state Co^+ reacting with propane has been shown to be due to the initial C-H bond activation transition state which is rate limiting, and is located only 0.11 eV below the Co^+/C_3H_8 asymptotic energy.[28] As a result, the vibrationally excited $CoC_3H_8^+$ complex which is initially formed can dissociate back to reactants or can be collisionally stabilized in strong competition with elimination channels. Under single collision conditions, Fisher and Armentrout (in ref 28) measured the efficiency for H_2 and CH_4 elimination channels to be 0.13 ± 0.05. This is approximately an order of magnitude larger than what we observe simply because, under the high-pressure conditions in our experiment, the elimination channels are competing with adduct formation.

(28) van Koppen, P. A. M.; Brodbelt-Lustig, J.; Bowers, M. T.; Dearden, D. V.; Beauchamp, J. L.; Fisher, E. R.; Armentrout, P. B. *J. Am. Chem. Soc.* **1991**, *113*, 2359; **1990**, *112*, 5663.

(29) In order to quantify the absolute rate coefficients, calibration reactions with known rates were studied. Reproducible but relatively low rate constants were obtained. The difference in the known and measured rates was found to depend on the mass of the neutral. The flow of the neutral entrained in the He buffer gas varies with the mass of the neutral.[20] An attempt to quantify this effect is in progress. However, the data taken to date indicate that the rate constants obtained with C_3H_8 will be low by about a factor of 2. For example, the rate of adduct formation for ground-state $Co^+ + C_3H_8$ which was measured to be 4.8×10^{-10} cm^3/s is actually a factor of 2 greater, 9.6×10^{-10} cm^3/s. The rate constants listed in Tables II and III have been obtained by multiplying the measured value by 2 to take this effect into account. The factor of 2 does not effect the interpretation of the results and conclusions made. The relative rates of reaction are reproducible to ±5% and this is what the interpretation of the results are based on.

(30) Tonkyn, R.; Ronan, M.; Weisshaar, J. C. *J. Phys. Chem.* **1988**, *92*, 92.

Table II. Effective $Co^+ + C_3H_8$ Bimolecular Rate Constants at 300 K, 1.75 Torr of He[a]

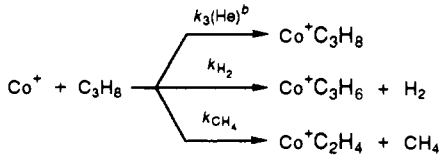

	k_3(He)[c]	k_{H_2}[c]	k_{CH_4}[c]	k_{tot}/k_L[d]	k_{H_2}/k_{CH_4}
Co^+ (a^3F, $3d^8$)	96	1.4	0.3	0.84	4.7
$(Co^+)^*$ (a^5F, b^3F, $4s3d^7$)	2.6	5.0	5.6	0.11	0.9
$k_{Co^+}/k_{(Co^+)^*}$	37	0.28	0.05		

[a] The accuracy of the absolute rate coefficient measurements is estimated to be within 30%.[20] The relative rate coefficient measurements, however, are much more accurate (±10%).[29] [b] Only He stabilization is important because of the low propane pressure. [c] Rate constants in units of 10^{-11} cm^3/s. [d] The Langevin rate constant, $k_L = 1.17 \times 10^{-9}$ cm^3/s.

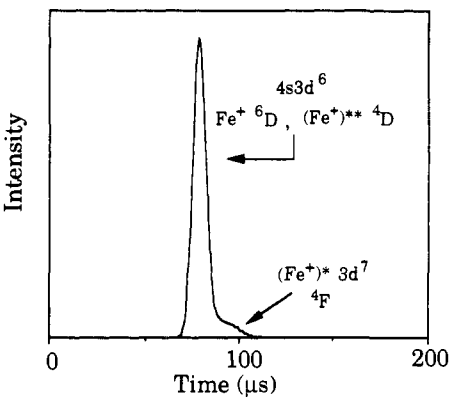

Figure 6. Fe^+ arrival time distribution (ATD), 300 K, 50 eV, Fe^+ from $Fe(CO)_5$. The excited ^4D and ground ^6D states have the same $4s3d^6$ electronic configuration with identical arrival time distributions. The ^4F state, however, has a $3d^7$ electronic configuration and an ATD distinct from the ^6D and ^4D states. Collisional deactivation of the ^4F state to the ^6D state gives rise to the tail at long times in the ATD. Without deactivation two base-line resolved peaks would be observed in the ATD analogous to Co^+ (see Figure 1).

That the H_2 and CH_4 elimination channels are greatly enhanced with the excited-state $(Co^+)^*$ reactant is clearly shown in Figure 5. This is apparently due to lower transition-state energies for elimination on the excited-state surface compared with the ground-state surface (lower relative to the respective reactant asymptotic energies). At first glance, this is a surprising result since the excited-state electrostatic well associated with Co^+-$(4s3d^7)\cdot C_3H_8$ is surely much shallower than the ground-state well, owing to the presence of the 4s electron. Consequently, the excited-state elimination transition state should be less stabilized by this well than the ground state. However, C–H or C–C bond activation by a metal ion with a singly occupied 4s orbital correlates to an antibonding orbital of the complex formed.[12,30] Formation of the fully inserted H–Co^+–C_3H_7 or CH_3–Co^+–C_2H_5 intermediates must therefore correlate to ground-state surfaces. Since these ground-state surfaces are at much lower energy, significant stabilization of the excited-state insertion transition state is expected. This enhances the H_2 and CH_4 eliminating channels for the excited-state $(Co^+)^*$ compared with those of ground-state Co^+.

It is interesting to note the enhancement of the CH_4 loss channel for excited-state $(Co^+)^*$ relative to ground-state Co^+. The $k(H_2)/k(CH_4)$ ratio is 4.7 for ground-state and 0.9 for excited-state Co^+ (Table II). The most plausible explanation for the dramatic increase in CH_4 elimination for excited-state Co^+ is that both initial C–C and initial C–H bond activation is occurring on the excited-state surface, while only initial C–H bond activation occurs on the ground-state surface.[31] The $k(H_2)/k(CH_4)$ ratio of 4.7

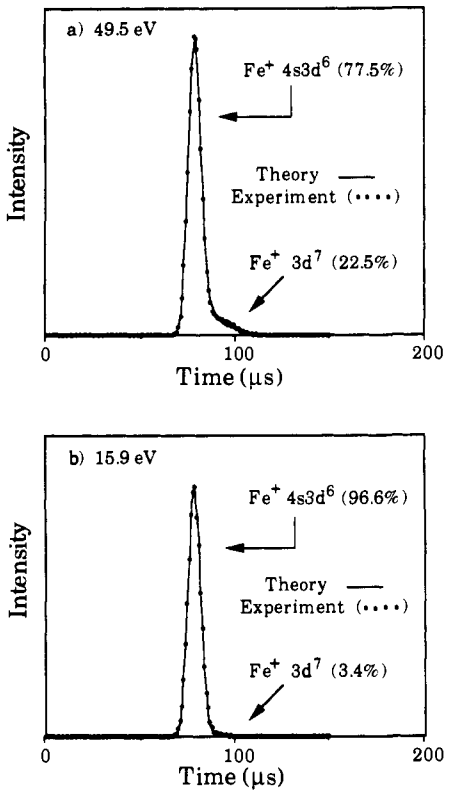

Figure 7. Theoretical and experimental ATDs for Fe^+ at (a) 49.5 and (b) 15.9 eV. The fraction of the $4s3d^6$ and $3d^7$ electronic state configurations, as well as the rate of deactivation of the ^4F state to the ^6D state, is obtained by theoretically fitting the ATDs.

for ground-state Co^+ is in good agreement with the results reported by Fisher and Armentrout (in ref 28) and Tonkyn et al.[30] The surface ionization experiment of Fisher and Armentrout produces 15% a^5F excited-state Co^+ and 85% a^3F ground-state Co^+. Under these conditions, the $k(H_2)/k(CH_4)$ ratio was found to be 3.3. This ratio, however, is very sensitive to the presence of excited-state Co^+. Correcting for the 15% excited-state contribution gives a ground-state branching ratio of 4.5 which is in essentially exact agreement with our results. Using laser vaporization to form the Co^+ ions, Tonkyn et al. found the $k(H_2)/k(CH_4)$ branching ratio to be 3.0. Laser vaporization does produce at least a few percent excited-state Co^+.[32] This percentage, however, depends on the experimental conditions. Correcting for a 5% excited-state contribution in these results, yields a ground-state branching ratio of 3.2, in fair agreement with the present results. The relatively large corrections for the excited-state population (especially in the surface ionization experiment) emphasize the fact that the excited-state contribution to reactivity studies of transition metal ions cannot be ignored.

IV. Electronic State Populations: $Fe^+ + C_3H_8$. A typical ATD of Fe^+ at 300 K and 50 eV is shown in Figure 6. Unlike the ATD for Co^+, where two base-line resolved peaks corresponding to ground- and excited-state Co^+ are observed, the Fe^+ ATD consists of a single peak with a slight tail. This peak is a composite of three electronic states, the ground state ^6D $4s3d^6$, the first excited state ^4F $3d^7$, and the second excited state ^4D $4s3d^6$. (Evidence for the production of higher lying electronic states of Fe^+ formed by EI on $Fe(CO)_5$ has been presented and is discussed below.[17,33])

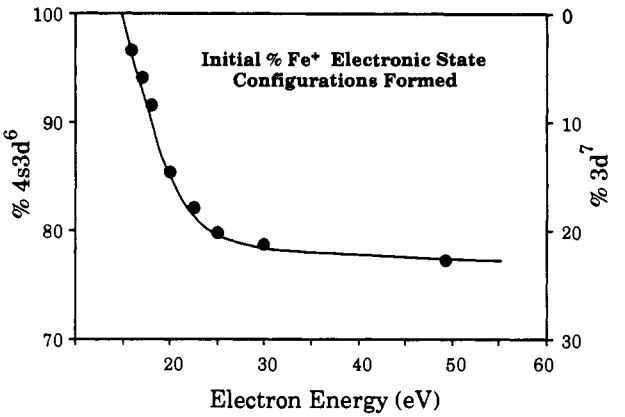

Figure 8. The initial % Fe^+ $4s3d^6$ and $3d^7$ electronic state configurations formed versus electron energy obtained from the theoretical fit to the Fe^+ ATDs. At 49.5 eV, 22.5% of the Fe^+ corresponds to the $3d^7$ configuration.

The ^4D and ^6D states have the same $4s3d^6$ electronic configuration with identical ATDs. The ^4F state, however, has a $3d^7$ configuration and, in the absence of deactivation, would yield an ATD peak similar to that of ground-state Co^+ and distinct from the ^6D and ^4D states. Collisional deactivation of the ^4F state to the ^6D state does occur, however, and gives rise to the observed tail at long times on the peak in Figure 6. As we decrease the electron energy, the tail on the Fe^+ ATD decreases owing to decreased ^4F state population.

A theoretical ATD can be calculated from the known transport properties[3a,34] of the ground and excited states of Fe^+. The fraction of the $4s3d^6$ and $3d^7$ electronic state configurations as well as the rate of deactivation of the ^4F state to the ^6D state are obtained by theoretically fitting the experimental ATDs. The theoretical fits to the experimental ATDs for Fe^+ formed by electron impact at 49.5 eV and 15.9 eV are shown in Figure 7. At 49.5 eV, the initial population of ^4F $3d^7$ electronic state was found to be 22.5%, and the deactivation rate constant was 9.5×10^{-13} cm^3/s. At 15.9 eV, the tail in the ATD due to the ^4F state is very nearly nonexistent, and the initial population of the ^4F state was determined to be 3.4%. The deactivation rate constant which is independent of the electron energy is again 9.5×10^{-13} cm^3/s. The theoretical fits to the experimental ATDs were very nearly exact at all electron energies, similar to the 15.9- and 49.5-eV data in Figure 7. The resulting initial population of the different Fe^+ electronic state configurations as a function of electron energy is shown in Figure 8.

It is more difficult to determine the relative populations of the ^6D ground state and ^4D second excited state since the states have the same $4s3d^6$ configuration and are not resolved in our ATD spectrum. However, we were able to determine the populations using kinetic information from our experiment. The analysis used is discussed here and in the next section on the kinetic analysis, since the determination of the populations and rate coefficients are interrelated.

Consider the relative clustering efficiencies of Fe^+ ^6D and ^4D with C_3H_8. Ordinarily, states containing a 4s electron are quite inefficient at clustering. The Co^+ b^3F state is an example. However, all our data, both kinetic and product ion ATDs at low eV, indicate that the Fe^+ ground state clusters efficiently. This result strongly indicates that there is a crossing of the closely spaced ($\Delta E \sim 6$ kcal/mol) ^4F and ^6D curves, which allows the Fe^+ ground state to enter the $Fe^+(^4F\ 3d^7)\cdot C_3H_8$ potential well where the adduct is more strongly bound (see Figure 9). Thus, although the Fe^+ ^6D ground state has a $4s3d^6$ configuration, it clusters with C_3H_8 efficiently, similar to the Co^+ a^3F $3d^8$ ground state.

(31) Initial C–H and C–C bond activation in the mechanism for H_2 and CH_4 elimination channels was initially proposed in the literature. See, for example: (a) References 1 and 24. (b) Armentrout, P. B.; Beauchamp, J. L. *J. Am. Chem. Soc.* **1981**, *103*, 784. (c) Larsen, B. S.; Ridge, D. P. *J. Am. Chem. Soc.* **1984**, *106*, 1912. (d) Byrd, G. D.; Burnier, R. C.; Freiser, B. S. *J. Am. Chem. Soc.* **1982**, *104*, 3565. (e) Hankinson, D. J.; Allison, J. *J. Phys. Chem.* **1987**, *91*, 5307. However, a very thorough recent study (ref 28) indicates unambiguously only initial C–H insertion occurs on the ground state surface.

(32) von Helden, G.; Kemper, P. R.; Bowers, M. T. Unpublished results.

(33) Oriedo, J. V. B.; Russell, D. H. *J. Phys. Chem.*, in press.

(34) Mason, E. A.; McDaniel, E. W. *Transport Properties of Ions in Gases*; Wiley and Sons: New York, 1988.

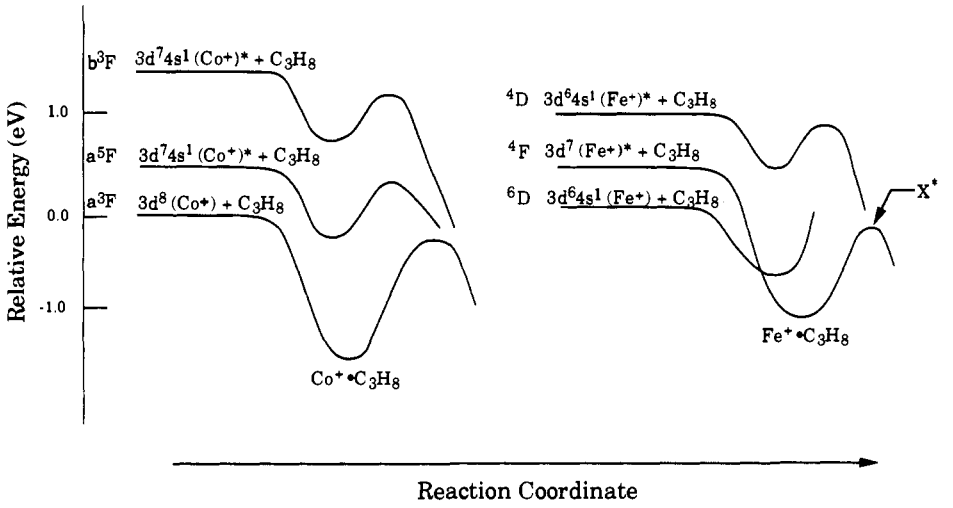

Figure 9. Schematic reaction coordinate diagrams for Co^+ and Fe^+ reacting with C_3H_8. For Fe^+ and ^4F excited state crosses the ^6D ground state yielding a common C–H insertion transition state, X*, for the two surfaces. In all cases the transition states correspond to initial C–H (ground states) or C–H/C–C (excited states) bond activation by the metal ion. See text.

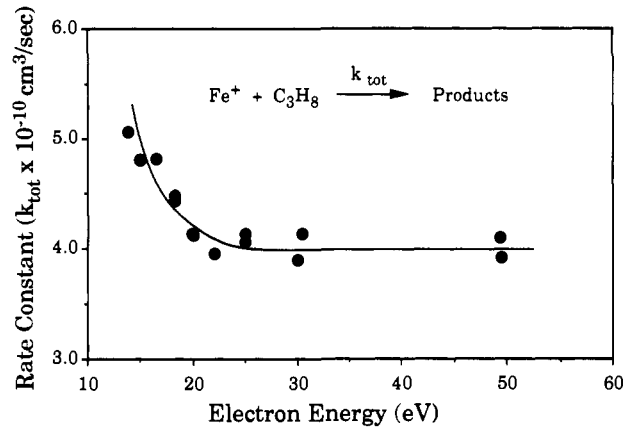

Figure 10. The total rate constant for Fe^+ reacting with C_3H_8 as a function of electron energy, at reaction times greater than 100 μs. At the lowest electron energy, only the ^6D ground state is present. As the electron energy is increased, the ^4D state is populated and a decrease in the rate of adduct formation is observed. The ^4F state has reacted away or has been deactivated for $t > 100$ μs.

This enhanced clustering does *not* occur with the Fe^+ ^4D $4s3d^6$ second excited state, since no low-lying $3d^7$ state is present. (The Fe^+ ^4P $3d^7$ state is 15.1 kcal/mol above the ^4D.) Thus, we expect the ^4D state to cluster similarly to the Co^+ 4s containing states (i.e., about 40 times less efficient than the ground state at these He pressures).

This difference in reactivity allows us to determine the ^6D and ^4D populations. The observed change in the clustering rate constant for ionizing electron energies near threshold to 50 eV, for reaction times greater than 100 μs, is shown in Figure 10 (complications due to clustering of the Fe^+ ^4F first excited state were avoided by observing the reaction at times greater than 100 μs when the ^4F state has either been deactivated or has reacted). Near threshold the electronic state population is essentially 100% ^6D ground state. As we increase the electron energy to 50 eV, the ^4D state is populated and the observed rate of reaction decreases by 23%. Above 50 eV, the populations should remain constant and no further change in the rate constant is observed. If the ^4D state forms no cluster, this would correspond to 23% ^4D in Fe^+ formed by 50-eV electron impact on $Fe(CO)_5$. In a more complete analysis, including the nonzero ^4D clustering rate constant, the small elimination channels and the small amount of cluster product from the ^4F state during deactivation indicate that 20 ± 3% ^4D state is initially formed at 50-eV electron energy. Since our ATD analysis (Figure 7a) shows that 22.5% Fe^+ ^4F is also formed at this electron energy, the initial % Fe^+ ^6D ground state is then calculated to be 57%.

The analysis so far has included only the three lowest Fe^+ states. Evidence does exist for the presence of higher energy states,[17,33] and we must evaluate their possible effects on our data. Oriedo and Russell[33] have recently used dissociative charge transfer ($(Fe^+)^*$ + $Fe(CO)_5$ → products) to gauge the range of internal energies in Fe^+ formed by electron impact in a low-pressure FT–ICR experiment. Assuming a Fe^+ ^6D ground-state population of ~50%, based on our work presented here and that of Armentrout and co-workers,[17] the FT–ICR Fe^+ state populations are estimated to be: ^4F, ~20%; ^4D + ^4P + ^2G, ~15%; states between 2.25 and 2.59 eV, ~5%; states between 2.76 and 3.34 eV, ~5%, and states greater than 3.72 eV, ~5%. Under multicollision conditions, however, Oriedo and Russell found that all the higher lying excited states (a^4P and higher) were deactivated except for one long-lived state lying approximately 2.84 eV above the ground state. This long-lived state is either a $4s^23d^5$ or $4s3d^6$ electronic configuration and comprises less than 5% of the total electronic state population. Therefore, only small amounts of highly excited Fe^+ exist in our high-pressure experiment.

Armentout and co-workers[17] have used $Fe^+ + O_2$ and $Fe^+ + (H/D)_2$ reaction cross sections to gauge Fe^+ ground- and excited-state populations. They also found states with energies equal to or higher than the Fe^+ ^4P $3d^7$ (1.64 eV above ground state); however, by comparison with known Fe^+ populations from surface ionization (SI), they determined that the *total* amount of *all* excited states above the ^4D state was less than 5% of the Fe^+ ionization. Their other state populations were estimated to be: ^6D ground state, ~40%; ^4F, ~16%; ^4D, ~40%. They also investigated the collisional deactivation of the high-energy state(s) (^4P or higher) and found them to deactivate, but at a rate much slower than the ^4F. This suggests that the high-energy state could be the ^4P, since a ^4P $3d^7$ → ^4D $4s3d^6$ deactivation/crossing could occur, but less efficiently than the ^4F $3d^7$ → ^6D $4s3d^6$ crossing, because of the larger energy difference (0.656 eV versus 0.248 eV).

The present ATD data allow us to say that no significant amount (<1–2%) of undeactivated Fe^+ with a $3d^7$ configuration exists after 100–200 μs in our experiment. This rules out the presence of all the higher lying $3d^7$ electronic state configurations (the ^2G, ^2P, ^2H, or ^2D states, 1.94–2.50 eV above ground state), since no $4s3d^6$ configuration states are available for crossing. A small amount (1–5%) of the excited Fe^+ ^4P $3d^7$ state with a deactivation rate slower by a factor of 2–5 than that of the ^4F could be hidden in the ATD. Thus, the presence of a few percent ^4P $3d^7$ in our experiment cannot be ruled out. This would be in agreement with Armentrout and co-workers' results.[17]

Our ATD results do not rule out the presence of high-energy $4s3d^6$ configuration states, since the corresponding ATD peak will

Table III. Effective $Fe^+ + C_3H_8$ Bimolecular Rate Constants at 300 K, 1.75 Torr of He[a]

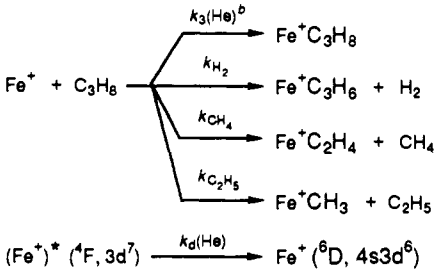

	$k_3(He)^c$	$k_{H_2}{}^c$	$k_{CH_4}{}^c$	$k_{C_2H_5}{}^c$	$k_d{}^d$	$k_{tot}/k_L{}^e$	k_{CH_4}/k_{H_2}
Fe^+ (^6D, $4s3d^6$)	48	0.60	1.50			0.42	2.5
$(Fe^+)^*$ (^4F, $3d^7$)	<20	20.8	21.8	9.4	9.5×10^{-13}	0.53	1.0
$(Fe^+)^{**}$ (^4D, $4s3d^6$)	~1.0	2.8	5.8	0.36		0.09	2.1
$k_{Fe^+}/k_{(Fe^+)^*}$	>2.5	0.03	0.07				
$k_{Fe^+}/k_{(Fe^+)^{**}}$	~40	0.21	0.26				

[a] The accuracy of the absolute rate coefficient measurements is estimated to be within 30%.[20] The relative rate coefficient measurements, however, are much more accurate (±10%).[29] [b] Only He stabilization is important because of the low propane pressure. [c] Rate constants in units of 10^{-11} cm^3/s. [d] Deactivation rate constant with helium buffer gas, in units of cm^3/s. [e] The Langevin rate constant, $k_L = 1.19 \times 10^{-9}$ cm^3/s.

be superimposed on the $^6D/^4D$ peak. However, as noted above, estimates of these state populations under multicollision conditions[33] range from ~0% to 5%. If a relatively small percentage of these highly excited $4s3d^6$ states are present, the consequences are as follows. First, the large energy available (2.59–3.72 eV) might open other reaction pathways; however, no products were found other than those known to come from the ^6D, ^4F, and ^4D states. Second, without a low-lying Fe^+ $3d^7$ state available for curve crossing, we do not expect these highly excited $4s3d^6$ states to cluster with C_3H_8, by analogy with the excited Co^+ $4s3d^7$ results. Thus, the elimination reactions appear to be the only pathways available to any Fe^+ states above the ^4D. From Oriedo and Russell's data it appears that if any highly excited Fe^+ states are present, they are of $4s3d^6$ configuration. From the above discussion, these states react similarly to the ^4D state if they react at all. As discussed for the $4s3d^7$ states of Co^+, mixing with the $3d^7$ surface allows for C–H or C–C bond activation to occur. Because of the large energy difference between the highly excited $4s3d^6$ states an the $3d^7$ states of Fe^+, state mixing is not probable. Elimination reactions may thus be very inefficient. This validates our analysis except to note that part (<5%) of our reported 20% ^4D population may, in fact, be other higher energy $4s3d^6$ states.

V. Kinetic Analysis: $Fe^+ + C_3H_8$. The analysis here is complicated. Three Fe^+ states react to cluster, eliminate (via three channels), and deactivate. In this section we describe the analysis used to calculate the individual rates. The next section discusses the results.

a. Fe^+ ^6D $4s3d^6$ Ground State. By working at the lowest usable electron energy (~14 eV nominal), we can largely eliminate the ^4F and ^4D states. The ATD spectra confirm this: at 14 eV the percent ^4F is ≲3%. The higher energy ^4D state population is presumably even smaller and we will assume it is negligible. We eliminate the small effect of ^4F reaction by only looking at rates and product distributions at long times when the ^4F has deactivated to the ^6D ground state. The total rate constant as a function of electron energy is shown in Figure 10 where a total rate constant of $5.1 \pm 0.4 \times 10^{-10}$ cm^3/s is obtained at our lowest eV. Figure 11 shows the corresponding product distributions where, at low eV, H_2 and CH_4 elimination comprise 1.4% and 3% of the total products, respectively. No C_2H_5 elimination is seen, and it is, in fact, an endothermic product. Clustering to form $Fe^+ \cdot C_3H_8$ thus accounts for ≳95% of the Fe^+ ground-state reaction. These rate coefficients are summarized in Table III.

b. Fe^+ ^4D $4s3d^6$ Second Excited State. By increasing the ionizing energy while still observing the reaction at long times, the effect of the ^4D state can be evaluated. The effects on the observed rate constant and product distribution are shown in Figures 10 and 11. As the ionizing energy increases from 14 to 50 eV, the total rate constant decreases by 23%, while the fraction

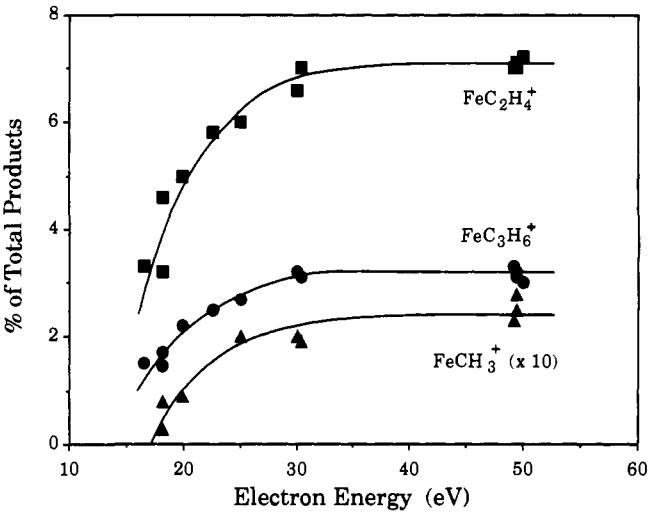

Figure 11. The percent of total products as a function of electron energy, for reaction times greater than 100 μs. At the lowest electron energy, only the ^6D ground state is present. As the electron energy is increased, the ^4D state is populated and an increase in the elimination product channels is observed. The ^4F state has reacted away or has been deactivated for $t > 100$ μs.

of elimination products increases to ~10% of the total products. Also, the C_2H_5 elimination channel is now present. As discussed above in section IV, we assume the ^4D state has a clustering rate about 2.5% that of ground-state Fe^+, by analogy with the excited $4s3d^7$ Co^+ states. In fact, the excited Fe^+ $4s3d^6$ states may cluster somewhat *less* efficiently owing to the larger Fe^+ ion size.[35] In any case, we expect the ^4D clustering rate constant to be small, and in this case comparison of the known Fe^+ ground-state elimination rate constants with those observed at 50 eV (when both ^6D ground state and ^4D states are present) allows a unique determination of the ^4D population and rate coefficients. These are listed in Table III.

c. Fe^+ ^4F $3d^7$ First Excited State. Analysis of the ^4F state begins with the initial state populations and the collisional deactivation rate. As discussed, by theoretically fitting the experimental Fe^+ ATDs, the collisional deactivation rate constant was determined to be 9.5×10^{-13} cm^3/s and the initial fraction of ^4F was determined to be 22.5% at 50-eV electron energy. The procedure used to extract the elimination and adduct formation rate coefficients involved calculating theoretically the observed

(35) Barnes, L. A.; Rosi, M.; Bauschlicher, C. W., Jr. *J. Chem. Phys.* **1990**, *93*, 609.

product distribution for Fe^+ (all states) reacting with C_3H_8 as a function of time. This requires an exact solution of the kinetic equations, details of which are given in the Appendix. Since the only unknowns are the ^4F reaction rate coefficients, matching the experimental and calculated product distributions at long times (no ^4F present) and at short times (^4F present) determined the ^4F rate constants. This fitting, however, is insensitive to the ^4F adduct formation rate constant since the total rate constant (which is the sum of adduct formation, elimination, and deactivation rate constants) is approximately equal to the deactivation rate constant (within 1%; see Appendix, section 2). Thus, the adduct formation rate constant of the ^4F state must be obtained in an alternate way. An upper limit is derived from the $Fe^+ \cdot C_3H_8$ product ATD. This ATD shows no observable adduct derived from a $3d^7$ electronic state configuration of Fe^+ (e.g., Fe^+ ^4F $3d^7$). From this we estimate the ^4F contributes less than 4% to the clustering channel. Together with the known initial ^4F population, this sets a limit of $k_3(He) < 20 \times 10^{-11}$ cm^3/s. The rate constants are summarized in Table III.

VI. Discussion of Reaction Rates: $Fe^+ + C_3H_8$. Reaction rate constants for the ^6D, ^4F, and ^4D states of Fe^+ with C_3H_8 at 300 K and 1.75 Torr of He are summarized in Table III. The major product under these conditions is adduct formation (96% for ground state Fe^+) being formed at 40% of the collision rate. These results are in good agreement with Tonkyn et al.[30] where the adduct was also found to be the major product (94% at 300 K and 0.75 Torr of He) being formed at 53% of the collision rate.

The rapid collisional deactivation of the Fe^+ ^4F state to the ground state, indicates that a curve crossing occurs in the Fe^+/He collisions. Our experimental data for Fe^+ reacting with propane is also consistent with a surface crossing of the ^4F state to the ground state, since relatively efficient ground-state adduct formation is found. However, the rate of adduct formation for ground-state Fe^+ reacting with C_3H_8 is a factor of 2 smaller than that of Co^+ ground state. This is not unexpected given the effectively reduced well depth of the $Fe^+C_3H_8$ complex relative to the Fe^+ ground-state asymptote since the bottom of the well diabatically correlates to the ^4F Fe^+ asymptote that lies 6 kcal/mol above the ^6D asymptote (see Figure 9). The surface crossing implies a common C–H and/or C–C bond activation transition state, X^*, for the ^4F and ^6D ground state Fe^+ reacting with propane (see Figure 9). Since we observe H_2 and CH_4 loss from ground-state Fe^+, X^* must lie below the ground-state Fe^+/C_3H_8 reactant energy. In a separate study, X^* was determined to be located only 0.07 eV below the asymptotic energy of the ground-state reactants.[36] The ^4F state lies 0.25 eV above ground-state Fe^+ and is therefore 0.32 eV above the transition state X^*. Thus, when the Fe^+ ^4F state reacts with C_3H_8 we expect (1) deactivation to Fe^+ ground state, (2) a large enhancement of the elimination channels, and (3) a decrease in the rate of adduct formation relative to that of the ground state due to competition with elimination channels. These expectations were all observed experimentally. The rate constant for adduct formation for the ^4F excited state is $<20 \times 10^{-11}$ cm^3/s, whereas the ground-state rate constant was found to be greater, 48×10^{-11} cm^3/s. The ^4F elimination channels are relatively efficient with rate constants of 20.8 and 21.8×10^{-11} cm^3/s for H_2 loss and CH_4 loss, respectively. The corresponding ^6D ground-state rate constants were 0.6 and 1.50×10^{-11} cm^3/s. Schultz and Armentrout[37] and Hanton, Noll, and Weisshaar[38] have measured the absolute cross section of the ^4F state relative to the ^6D state of Fe^+ reacting with C_3H_8 as a function of collision energy under single collision conditions. In both studies the ^4F state was found to be more reactive with regard to elimination than the ^6D state, in agreement with our results. However, Hanton et al. obtain efficiencies for CH_4 elimination (at 0.24 eV kinetic energy) which are an order of magnitude less than our results (at thermal energy) for both the ^6D and the ^4F states. A lower reaction efficiency with increasing energy (or temperature) is expected for a mechanism which involves complex formation, but an order of magnitude decrease at 0.24 eV kinetic energy seems a bit large. Schultz and Armentrout measured these rates at 0.05 eV kinetic energy and find the efficiencies for CH_4 elimination to be 6–10% for the ^4F state and 5% for the ^6D state which are in reasonable agreement with our results which are 18% and 1%, respectively. For H_2 elimination, Schultz and Armentrout find the efficiency to be 6.1% for the ^4F state and 1.6% for the ^6D state, again in reasonable agreement with our results which are 17% and 0.5%, respectively. The relatively large efficiencies observed for the ^4F state in our results may be attributed to the multicollision conditions in our experiment compared with the single collision conditions in the experiment of Schultz and Armentrout. Once the vibrationally excited $Fe^+(^4F)C_3H_8$ complex is formed, a collision may remove just enough energy to prevent decomposition back to reactants and not enough energy to stabilize the complex (stabilization would require a 0.32-eV drop in energy (see Figure 9)). Since crossing over to the $Fe^+(^6D)C_3H_8$ surface may not be facile at this energy, H_2 and CH_4 elimination from the vibrationally excited $Fe^+(^4F)C_3H_8$ complex might be very efficient, more so than under single collision conditions where decomposition back to reactants competes with the elimination channels.

The ^4D $4s3d^6$ second excited state of Fe^+ forms an adduct less efficiently than either the ^6D $4s3d^6$ ground state or ^4F $3d^7$ first excited state, and the elimination channels are enhanced relative to the ^6D state but less efficient than the ^4F state. The decrease in clustering is due to the presence of the 4s electron, as already discussed. The fact that the elimination rate constants for the ^4D state are between those of the ground state and the ^4F state suggests that the insertion transition state(s) on the surface correlating to Fe^+ ^4D is between 0.07 eV and 0.32 eV below the $Fe^+(^4D) + C_3H_8$ asymptotic energy.

The ratio for H_2 and CH_4 elimination, $k_{CH_4}/k_{H_2} = 2.5$, for ground-state Fe^+ reacting with C_3H_8 is in nearly exact agreement with Tonkyn et al.[30] and Armentrout et al.,[16,36] who found this ratio to be 2.2 and 2.8, respectively. Even though surface ionization in Armentrout's experiment and laser vaporization in Tonkyn's experiment will both produce some ^4F excited-state Fe^+, rapid collisional deactivation to ground-state Fe^+ will allow for pure ground-state Fe^+/C_3H_8 cross sections to be obtained without any contribution from the excited state. Near exact agreement between all three experiments is therefore quite satisfying.

Conclusion

Using electronic state chromatography we have determined the electronic state populations for Co^+ and Fe^+ as a function of ionizing energy. Reaction rates of state-selected Co^+ and Fe^+ ions reacting with propane were determined for adduct formation as well as for H_2 and CH_4 elimination channels. For Co^+, adduct formation at 1.75 Torr of He pressure is the dominant product of the ^3F $3d^8$ ground state, with only small amounts of elimination products observed. The Co^+ ^5F and ^3F $4s3d^7$ excited states react with very similar rate constants and show greatly reduced clustering (due to the repulsive 4s electron) and enhanced elimination channels. For ground-state Fe^+ ^6D $4s3d^6$, adduct formation is again dominant, despite the 4s electron, owing to a crossing of the ground state to the Fe^+ ^4F $3d^7$ low-lying first excited state where the adduct is more strongly bound. The Fe^+ ^4D $4s3d^6$ second excited state and the Co^+ a^5F and b^3F $4s3d^7$ excited states react very similarly. In each instance adduct formation is strongly reduced relative to the ground state and elimination reactions enhanced. The Fe^+ ^4F first excited state was collisionally deactivated to the ^6D ground state. The ^4F state also showed the largest H_2 and CH_4 elimination rates. Presumably this is due to an efficient coupling of the electronic energy into the reaction. Detailed kinetic analysis allowed quantitative determination of electronic state populations and rate constants for all observed reaction channels.

Acknowledgment. The support of the National Science Foundation under Grant CHE91-19752 is gratefully acknowl-

(36) van Koppen, P. A. M.; Bowers, M. T.; Fisher, E. R.; Armentrout, P. B. To be published.
(37) Schultz, R. H.; Armentrout, P. B. To be published.
(38) Hanton, S. D.; Noll, R. J.; Weisshaar, J. C. To be published.

edged. We also wish to thank Professor Dave Russell, Mr. Vincent Oriedo, and Professors Peter Armentrout and Jim Weisshaar for communicating results prior to publication and for several useful discussions. Finally, we wish to acknowledge Gert von Helden for writing the arrival time peak shape fitting program used to determine Fe^+ $3d^64s^1$ and $3d^7$ populations and the $3d^7$ to $3d^64s^1$ deactivation rate constant.

Appendix: Solution of Kinetic Equations for $Fe^+ + C_3H_8$

In order to calculate the theoretical product distributions, the kinetics of each state must be solved. In the derivation "**" refers to the ^4D second excited state, "*" to the ^4F first excited state, and no asterisks to the ground state.

(1) For the ^4D $4s3d^6$ second excited state, $(Fe^+)^{**}$, it is assumed that no deactivation occurs (analogous the $4s3d^7$ excited states of Co^+). This implies that the fractional decrease $(Fe^+)^{**}/(Fe^+)_0^{**}$ of this state is a simple exponential decay given in eq A1a. The total products, $(P^+)^{**}$ and the elimination products, $(P^+)_e^{**}$, formed as a function of time are given in eqs A1b and A1c, respectively.

$$(Fe^+)^{**} = (Fe^+)_0^{**}e^{-k_{tot}^{**}t} \qquad k_{1ol}^{**} = k_e^{**} + k_a^{**} \tag{A1a}$$

$$(P^+)^{**} = (Fe^+)_0^{**}(1 - e^{-k_{tot}^{**}t}) \tag{A1b}$$

$$(P^+)_e^{**} = (Fe^+)_0^{**}(k_e^{**}/k_{1ol}^{**})(1 - e^{-k_{tot}^{**}t}) \tag{A1c}$$

In these equations, k_e^{**}, k_a^{**}, and k_{1ol}^{**} correspond to the rate constants for elimination, adduct formation, and the total rate constant for the ^4D second excited state reacting with propane. The rate constants have units of s^{-1} and are equal to the bimolecular rate coefficient times the reactant concentration ($k_e^{**} = k_{H_2}(C_3H_8) + k_{CH_4}(C_3H_8)$ and $k_a^{**} = k_3(He)(C_3H_8)$).

(2) For the ^4F first excited state $(Fe^+)^*$, rapid deactivation to the ground state occurs. The fractional decrease $(Fe^+)^*/(Fe^+)_0^*$ for this state is again a simple exponential decay given in eq A2a. In this case, however, k_{1ol}^*, which is the sum of the rates of deactivation, elimination, and adduct formation, can be approximated by the rate of deactivation k_d^* (bimolecular deactivation rate times the He concentration). The elimination products, $(P^+)_e^*$, formed as a function of time are given in eq A2b.

$$(Fe^+)^* = (Fe^+)_0^* e^{-k_{tot}^*t} \qquad k_{1ol}^* = k_a^* + k_e^* + k_d^* \approx k_d^* \tag{A2a}$$

$$(P^+)_e^* = (Fe^+)_0^*(k_e^*/k_{1ol}^*)(1 - e^{-k_{tot}^*t}) \tag{A2b}$$

For reaction times greater than 100 μs, the ^4F state has been completely deactivated and the products formed prior to deactivation are constant and independent of time, eq A3.

$$(P^+)_e^* = (Fe^+)_0^*(k_e^*/k_d^*) = \text{constant} \tag{A3}$$

(3) The ^6D ground state reacts away to form the adduct and eliminate H_2 and CH_4 but is produced in the deactivation of the ^4F state as shown in eq A4, the solution to which is given in eq A5.

$$d(Fe^+)/dt = -k_{1ol}(Fe^+) + k_d^*(Fe^+)^* \tag{A4}$$

$$(Fe^+) = (Fe^+)_0e^{-k_{tot}t} + \frac{(Fe^+)_0^*k_d^*}{k_{1ol} - k_d^*}[e^{-k_d^*t} - e^{-k_{tot}t}] \tag{A5}$$

The total products for ground-state Fe^+ reacting with propane are calculated using expression A6 which has the solution given

$$d(P^+)/dt = k_{1ol}(Fe^+) \tag{A6}$$

by expression A7. The elimination products, $(P^+)_e$, formed from ground-state Fe^+ as a function of time are given in eq A8. Under our experimental conditions, $k_{1ol} \leq k_d^*/200$ and $k_{1ol} - k_d^* \approx -k_d^*$. In addition, for reaction times, $t > 10^{-4}$ s, $e^{-k_d^*t} < 10^{-3}$ and eqs A7 and A8 simplify to expressions A9 and A10, respectively.

$$(P^+) = (Fe^+)_0(1 - e^{-k_{tot}t}) + \frac{(Fe^+)_0^*k_d^*k_{1ol}}{k_{1ol} - k_d^*}\left[\frac{(1 - e^{-k_d^*t})}{k_d^*} - \frac{(1 - e^{-k_{tot}t})}{k_{1ol}}\right] \tag{A7}$$

$$(P^+)_e = (Fe^+)_0\frac{k_e}{k_{1ol}}(1 - e^{-k_{tot}t}) + \frac{(Fe^+)_0^*k_d^*k_e}{k_{1ol} - k_d^*}\left[\frac{(1 - e^{-k_d^*t})}{k_d^*} - \frac{(1 - e^{-k_{tot}t})}{k_{1ol}}\right] \tag{A8}$$

$$(P^+) = [(Fe^+)_0 + (Fe^+)_0^*](1 - e^{-k_{tot}t}) - (Fe^+)_0^*(k_{1ol}/k_d^*) \tag{A9}$$

$$(P^+)_e = [(Fe^+)_0 + (Fe^+)_0^*]\frac{k_e}{k_{1ol}}(1 - e^{-k_{tot}t}) - (Fe^+)_0^*\frac{k_e}{k_d^*} \tag{A10}$$

At this point, the total products eliminated from all three electronic states of Fe^+ reacting with propane can be calculated as a function of reaction time. The elimination rate constant of the ^4F state, k_e^*, is used as the only variable parameter to fit the experimental data.

Communications to the Editor

In Situ Chemisorption-Induced Reordering of Oxidatively Disordered Pd(100) Electrode Surfaces

John R. McBride, Jane A. Schimpf, and Manuel P. Soriaga*,†

Department of Chemistry, Texas A&M University College Station, Texas 77843

Received September 11, 1992

The regeneration of ordered, well-defined electrode surfaces outside an ultra-high vacuum environment is of utmost concern in electrochemical surface science. Four methods have been suggested in the past.[1-5] Three[1-4] require high-temperature treatments outside the electrochemical cell. The fourth method,[5] based upon microscopic electropolishing, is limited to reactive metals. Recently, we discovered that an oxidatively disordered Pd(111) surface could be reordered under purely electrochemical conditions.[6,7] The reordering is based upon the formation of a stable, highly ordered iodine overlayer when a Pd(111) single-

* Author to whom correspondence should be addressed.
† Presidential Young Investigator.

(1) Clavilier, J. *J. Electroanal. Chem.* **1980**, *107*, 211.
(2) Motoo, S.; Furuya, N. *J. Electroanal. Chem.* **1984**, *172*, 339.
(3) Wieckowski, A.; Schardt, B. C.; Rosasco, S. D.; Stickney, J. L.; Hubbard, A. T. *Inorg. Chem.* **1984**, *23*, 565.
(4) Zurawski, D.; Rice, L.; Hourani, M.; Wieckowski, A. *J. Electroanal. Chem.* **1987**, *230*, 221.
(5) Stickney, J. L.; Villegas, I.; Ehlers, C. B. *J. Am. Chem. Soc.* **1989**, *111*, 6473.
(6) Rodriguez, J. F.; Bothwell, M. E.; Cali, G. J.; Soriaga, M. P. *J. Am. Chem. Soc.* **1990**, *112*, 7392.
(7) Cali, G. J.; Berry, G. M.; Bothwell, M. E.; Soriaga, M. P. *J. Electroanal. Chem.* **1991**, *297*, 523.

0002-7863/92/1514-10950$03.00/0